Supplement of Atmos. Meas. Tech., 9, 1313–1324, 2016
http://www.atmos-meas-tech.net/9/1313/2016/
doi:10.5194/amt-9-1313-2016-supplement

Supplement of

Re-evaluating the Frankfurt isothermal static diffusion chamber for ice nucleation

J. Schrod et al.

Correspondence to: Erik S. Thomson (erik.thomson@chem.gu.se)

1 Repeated wafer tests

In the table below the raw data and calculated relative and weighted errors for repetitious tests of wafers are presented. Eighteen wafers were measured with between two and ten repetitions at eight temperature and saturation conditions (T, RH$_i = -15\,°\mathrm{C}$, $110\,\%$; $-20\,°\mathrm{C}$, $120\,\%$; $-25\,°\mathrm{C}$, $119\,\%$; $-25\,°\mathrm{C}$, $126\,\%$; $-30\,°\mathrm{C}$, $130\,\%$; $-30\,°\mathrm{C}$, $132\,\%$; $-32\,°\mathrm{C}$, $127\,\%$; $-32\,°\mathrm{C}$, $134\,\%$). This series of measurements resulted in 226 individual measurements, representing 87 wafer–saturation condition subsets. One wafer, saturation condition subset represents a single wafer repeatedly measured at a single saturation condition. For example, the measurement of wafer #1 at -15 °C and RH$_i$=110 % was repeated three times (see table below).

Relative error E_R is the percentage represented by the standard deviation σ_i of the mean INP counts $\overline{INP}_i$ per subset i. Thus for n repetitions per wafer within a subset

$$\overline{INP}_i = \frac{\sum_1^n INP}{n}, \tag{1}$$

where INP is the number of counts for an individual repetition and,

$$E_R = \frac{\sigma_i}{\overline{INP}_i} \times 100. \tag{2}$$

The weighted error E_W is the relative error normalized by the mean INP counts relative to the total INP counts for all subsets $\overline{INP}_{all}$, where

$$\overline{INP}_{all} = \sum_{i=1}^{87} \overline{INP}_i \text{ and} \tag{3}$$

$$E_W = \frac{\overline{INP}_i}{\overline{INP}_{all}} E_R. \tag{4}$$

A total weighted error is calculated and presented at the conclusion of the table and within the text by summing the contributions from all of the individual subsets. In this case we have treated all of the available data and made no attempt to eliminate outliers, etc. We have chosen this approach in an attempt to maintain the broadest interpretation of reproducibility and to ensure wafers with low total counts cannot skew the error to be very large given small changes in absolute count. However, in other measurement contexts (e.g., a subset of the analyzed thermodynamic conditions) it may be valuable to re-examine and/or use some subset of the data. Thus we provide the entirety of the data set below.

Wafer	T (°C), RH$_i$ (%)	Counts (INP)	Relative Error ($\%$)	Weighted Error ($\%$)
1	-15, 110	0	undefined	0
		0	(0)	
		0		
2	-15, 110	0	undefined	0
		0	(0)	
		0		
1	-20, 120	11	28.8	0.03
		20		
		16		
Wafer	T (°C), RH$_i$ (%)	Counts (INP)	Relative Error ($\%$)	Weighted Error ($\%$)

Wafer	T (°C), RH$_i$ (%)	Counts (INP)	Relative Error ($\%$)	Weighted Error ($\%$)
2	-20, 120	24	21.9	0.04
		37		
		29		
3	-20, 120	20	28.1	0.02
		13		
		12		
		14		
		9		
		10		
		9		
		11		
		12		
		12		
18	-20, 120	24	23.7	0.02
		17		
		17		
		13		
		13		
		13		
		13		
		14		
		13		
		15		
1	-25, 119	3	20.2	0.004
		4		
2	-25, 119	90	9.5	0.06
		103		
3	-25, 119	3	91.5	0.05
		14		
4	-25, 119	0	0	0
		0		
5	-25, 119	16	141.4	0.07
		0		
6	-25, 119	4	47.1	0.009
		2		
7	-25, 119	1	94.3	0.02
		5		
8	-25, 119	3	20.2	0.004
		4		
9	-25, 119	1	47.1	0.004
		2		
10	-25, 119	0	141.4	0.004
		1		
11	-25, 119	0	0	0
		0		
12	-25, 119	5	94.3	0.02
		1		
13	-25, 119	2	0	0
Wafer	T (°C), RH$_i$ (%)	Counts (INP)	Relative Error ($\%$)	Weighted Error ($\%$)

Wafer	T (°C), RH$_i$ (%)	Counts (INP)	Relative Error ($\%$)	Weighted Error ($\%$)
		2		
14	-25, 119	0 1	141.4	0.004
15	-25, 119	2 9 13	69.6	0.04
16	-25, 119	9 31 41	60.6	0.1
1	-25, 126	71 82	10.2	0.04
2	-25, 126	230 220	3.1	0.04
3	-25, 126	93 53	38.7	0.2
4	-25, 126	28 86	72.0	0.3
5	-25, 126	9 55 20	85.8	0.2
6	-25, 126	33 57	37.7	0.1
7	-25, 126	45 105	56.6	0.3
8	-25, 126	25 19 64	67.9	0.2
9	-25, 126	9 7	17.7	0.009
10	-25, 126	154 123	15.8	0.1
11	-25, 126	20 10	47.1	0.04
12	-25, 126	159 133	12.6	0.1
13	-25, 126	19 22	10.3	0.01
14	-25, 126	10 8	15.7	0.009
15	-25, 126	93 68 103	20.5	0.1
16	-25, 126	168 210 140	20.4	0.2
17	-25, 126	33 22 25	12.1	0.02
Wafer	T (°C), RH$_i$ (%)	Counts (INP)	Relative Error ($\%$)	Weighted Error ($\%$)

Wafer	T (°C), RH$_i$ (%)	Counts (INP)	Relative Error ($\%$)	Weighted Error ($\%$)
		26		
		26		
		27		
		23		
		25		
		30		
		27		
18	-25, 126	18	7.1	0.008
		17		
		19		
		16		
		18		
		16		
		18		
		17		
		18		
		20		
1	-30, 130	150	16.6	0.2
		190		
2	-30, 130	240	2.9	0.04
		250		
5	-30, 130	130	51.1	0.3
		61		
6	-30, 130	40	47.1	0.2
		80		
7	-30, 130	187	29.2	0.4
		254		
8	-30, 130	12	62.5	0.06
		9		
		28		
10	-30, 130	412	3.9	0.1
		390		
11	-30, 130	113	20	0.1
		85		
12	-30, 130	140	0.5	0.004
		139		
13	-30, 130	135	3.2	0.03
		129		
14	-30, 130	52	10.2	0.03
		45		
15	-30, 130	201	16.7	0.2
		182		
		154		
		173		
		184		
		144		
		255		
		188		
Wafer	T (°C), RH$_i$ (%)	Counts (INP)	Relative Error ($\%$)	Weighted Error ($\%$)

Wafer	T (°C), RH$_i$ (%)	Counts (INP)	Relative Error (%)	Weighted Error (%)
		163		
		192		
18	-30, 130	43	10.9	0.02
		41		
		35		
		34		
		33		
		33		
		33		
		32		
		35		
1	-30, 132	430	1.6	0.04
		440		
2	-30, 132	530	34.9	0.9
		320		
4	-30, 132	702	8.0	0.4
		786		
5	-30, 132	346	0.8	0.02
		350		
7	-30, 132	319	2.8	0.05
		332		
9	-30, 132	49	44.5	0.2
		94		
10	-30, 132	360	0.6	0.01
		357		
11	-30, 132	195	23.2	0.24
		140		
13	-30, 132	180	7.9	0.08
		161		
14	-30, 132	93	1.5	0.009
		91		
1	-32, 127	400	0	0
		400		
2	–32, 127	330	2.2	0.04
		320		
3	–32, 127	160	26.2	0.2
		110		
4	-32, 127	95	23.4	0.1
		68		
5	-32, 127	8	0	0
		8		
6	–32, 127	51	32.1	0.1
		81		
7	-32, 127	204	2.7	0.04
		212		
8	–32, 127	27	32.3	0.07
		43		
Wafer	T (°C), RH$_i$ (%)	Counts (INP)	Relative Error (%)	Weighted Error (%)

Wafer	T (°C), RH$_i$ (%)	Counts (INP)	Relative Error ($\%$)	Weighted Error ($\%$)
9	-32, 127	19 3	102.9	0.07
10	-32, 127	282 240	11.4	0.2
11	-32, 127	31 16	45.1	0.07
12	–32, 127	101 60	36.0	0.2
13	-32, 127	23 50	52.3	0.1
14	-32, 127	12 13	5.7	0.004
1	-32, 134	1100 1400	17.0	1.3
2	-32, 134	1150 900	17.3	1.1
4	-32, 134	1340 1900	24.4	2.5
5	-32, 134	741 536	22.7	0.9
6	-32, 134	895 1108	15.0	0.9
7	-32, 134	475 412	10.0	0.3
10	-32, 134	701 610	9.8	0.4
12	-32, 134	525 729	23.0	0.9
13	-32, 134	250 251	0.3	0.004
14	-32, 134	235 160	26.9	0.3
				$\sum = 16.1 \sim 20$
Wafer	T (°C), RH$_i$ (%)	Counts (INP)	Relative Error ($\%$)	Weighted Error ($\%$)

2 Saharan dust event

On April 16, 2015 a Saharan dust event was observed at the Taunus Observatory, Mt. Kleiner Feldberg (826 m msl, 50.221879° N, 8.446297° E). Figures 1 and 2 show the temporal evolution of the dust transport event in six hour increments. In Fig. 1 (a) and (b) the dust layer is primarily west of the Spanish and French coast and by 00 UTC on April 16 (Fig. 1 (c)) dust begins to pervade wide areas of central Europe. Figures 2 (d), (e) and (f) confirm that dust is present throughout the entire day, albeit within the RGB product the dust layer is superimposed with cold thick high-level clouds (red) and low-level clouds (yellow) and thus is not always clearly visible.

Figure 3 is the BSC-DREAM8b (vid BSC-DREAM8b ref., and Basart et al., 2012) modeled vertical profile of dust on April 16, 2015 above Taunus Observatory. It highlights that dust was present throughout the day, even in the lowest kilometer of the atmosphere. Thus it is reasonable to conclude that atmospheric samples taken at Taunus Observatory on April 16, 2015 included Saharan dust. Back trajectories from 12 UTC April 16, 2015 computed using HYSPLIT (Draxler and Rolph, 2015; Rolph, 2015) and arriving at the Taunus Observatory, confirm the observation that the local air mass advanced from the Saharan region (Fig. 4).

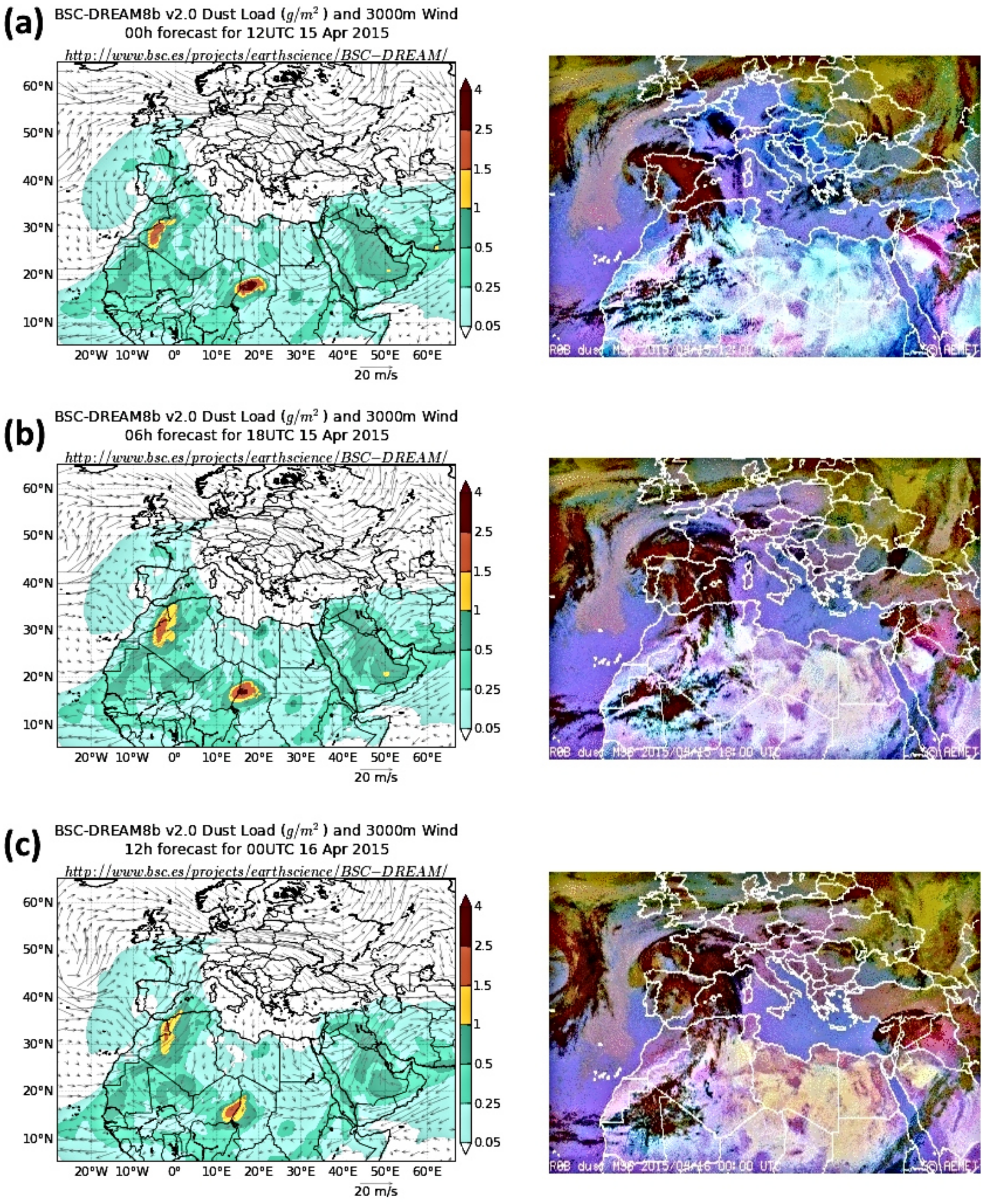

Figure 1. Temporal evolution of the Saharan dust event from (a) 12 UTC April 15, 2015 to (c) 00 UTC April 16, 2015. The lefthand panels show the dust load (g/m^2, calculated using BSC-DREAM8b), while the right-hand panels show the EUMETSAT RGB dust product, with the intensity of the magenta corresponding to dust intensity.

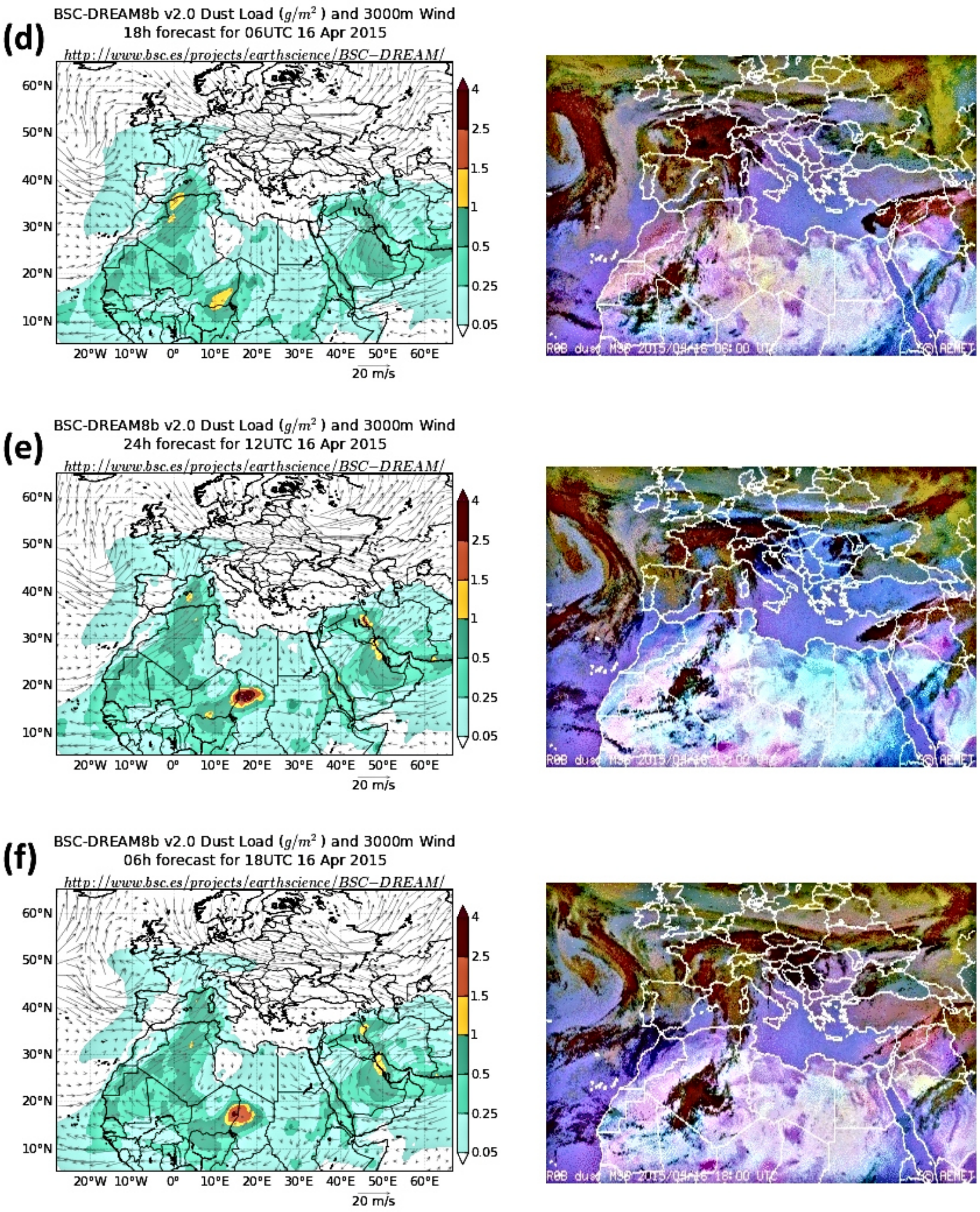

Figure 2. Continuation of Fig. 1's temporal evolution of the Saharan dust event from (d) 06 UTC April 1, 2015 to (f) 18 UTC April 16, 2015. Again the lefthand panels show the dust load (g/m^2, calculated using BSC-DREAM8b), while the righthand panels show the EUMETSAT RGB dust product, with the intensity of the magenta corresponding to dust intensity.

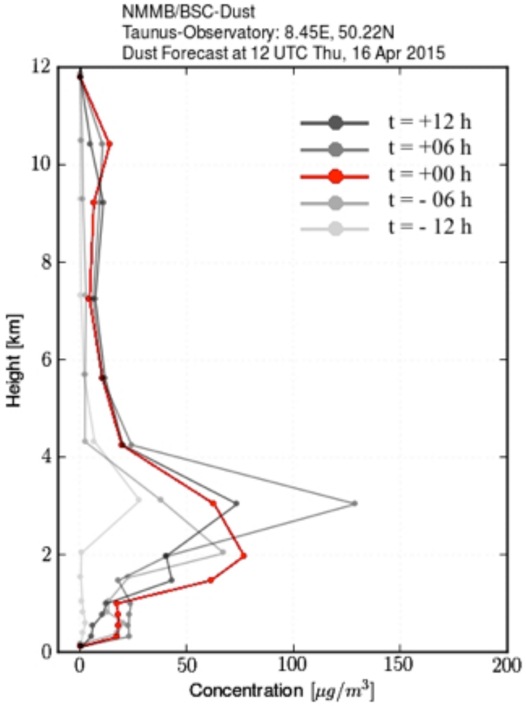

Figure 3. Vertical profile of dust concentration above Taunus Observatory on April 16, 2015 calculated using BSC-DREAM8b.

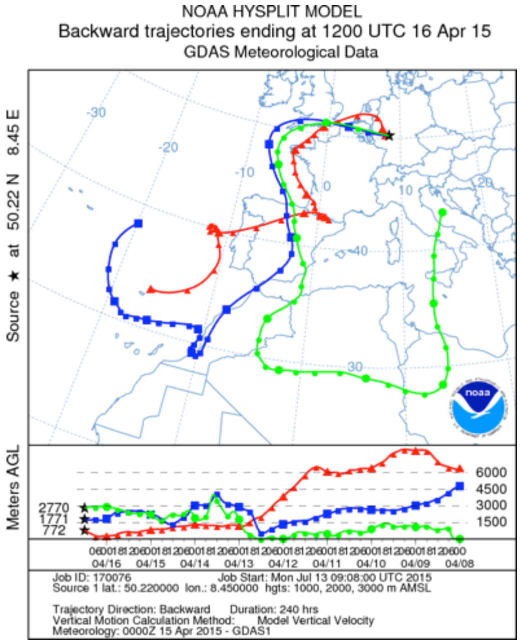

Figure 4. Back trajectories originating from Taunus Observatory at 1000 m (red), 2000 m (blue) and 3000 m (green) amsl. Trajectories were initiated at 12 UTC April 16 2015 and run for 240 hours.

References

Basart, S., Pérez, C., Nickovic, S., Cuevas, E., and Baldasano, J.: Development and evaluation of the BSC-DREAM8b dust regional model over Northern Africa, the Mediterranean and the Middle East, Tellus B, 64, 2012.

BSC-DREAM8b: Data and/or images from the BSC-DREAM8b (Dust REgional Atmospheric Model) model, operated by the Barcelona Supercomputing Center (http://www.bsc.es/projects/earthscience/BSC-DREAM/).

Draxler, R. R. and Rolph, G. D.: HYSPLIT (HYbrid Single-Particle Lagrangian Integrated Trajectory) Model access via NOAA ARL READY Website (http://ready.arl.noaa.gov/HYSPLIT.php), NOAA Air Resources Laboratory, Silver Spring, MD, 2015.

Rolph, G. D.: Real-time Environmental Applications and Display sYstem (READY) Website (http://ready.arl.noaa.gov), NOAA Air Resources Laboratory, Silver Spring, MD, 2015.